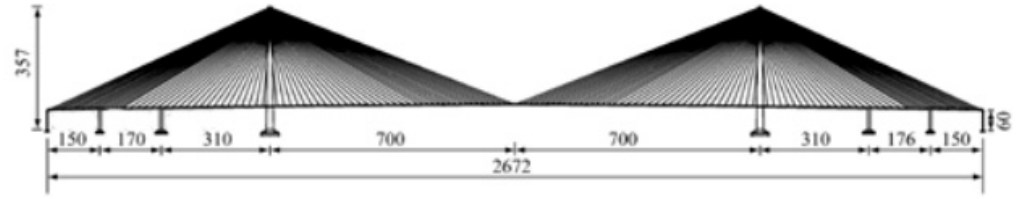

Fig. (1). Elevation View of Original Bridge (Unit: mm).

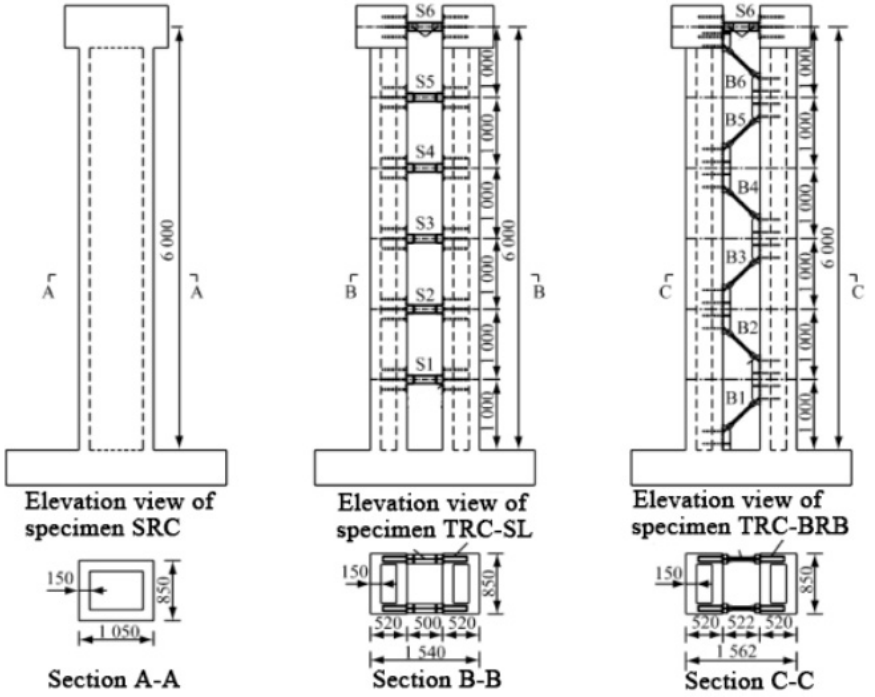

Fig. (2). Section and Elevation View of Specimen (Unit: mm).

Fig. (3). Pictures of Specimen.

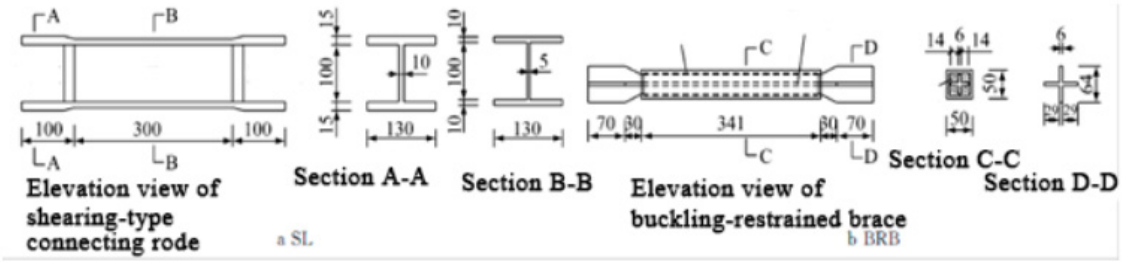

Fig. (4). Geometric Graphic of Energy Dissipation Components (Unit: mm).

the steel plate of core board freely extend along the axial direction, so as to reduce the shear force transfer between core board and sleeve. The thickness of steel plate used in core board is 6mm, the length keeps same along the brace, and the width is gradually and gently enlarged in the bottom.

4. TEST METHODS

Since the real quality of these three specimens is quite heavy, it is difficult for the crane to hang and move them. So in the test, the pouring is directly conducted by segmentation on the test rig so as to complete the production of specimen. In order to imitate the 25KN axial force given by the topside structure, the method is to design a reinforced concrete mass block on the top of specimen. The quasi-static loading is adopted in the test. The base is fixed on the test rig through four foundation bolts. Then MTS servo system hydraulic actuator exerts a low cyclic loading in a horizontal direction. The Max thrust force exerted by the actuator is 1500KN, the Max pulling force is 900KN and the Max stroke of displacement is 250mm, which equals that there happens a drift rate (ratio of the horizontal displacement of pier top to the loading height of pier column) of 4.2% on the pier top.

The loading mode of full displacement control is adopted in the test. The specific loading scheme is shown in Fig. (**5**). When the loading displacement level is before 30mm, there is 5mm progressively increased level by level starting from the initial 5mm. after 30mm, 10mm is progressively increased until the longitudinal bar in pier column breaks. To facilitate the research on strength degradation of specimen, the loading frequency for repeating each displacement level is set as three times.

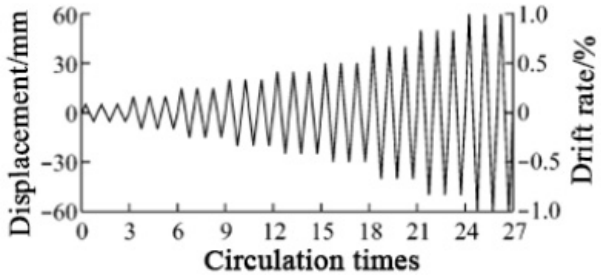

Fig. (5). Loading Scheme.

The transverse displacement of specimen is obtained by the displacement meter installed at each height. The strain value when the concrete cracks can be achieved by sticking the strain gauges on the steel bar and concrete surface and the energy dissipation component surface at the bottom of specimen. The occurrence of yield steel bar and energy dissipation component can be judged by means of the tested strain values. The average shearing deformation value γ of shearing-type connecting rod can`t be directly achieved, but the changes in value of diagonal length of rectangular connecting rod can be calculated by means of formula (1). The changes in value of diagonal length of connecting rod can be directly tested by the two displacement meters set along the diagonal direction. As is shown in Fig. (**6**), it is the geometrical relationship of average shearing deformation computation.

$$\gamma = \frac{(\Delta d_1 - \Delta d_2)\sqrt{a^2 + b^2}}{2ab} \quad (1)$$

In this formula: Δd1 = d′1-d1, Δd2 = d′2-d2, are respectively the value changes of two diagonal lengths. The lengths of both sides of rectangular connecting rod are respectively set as A and B.

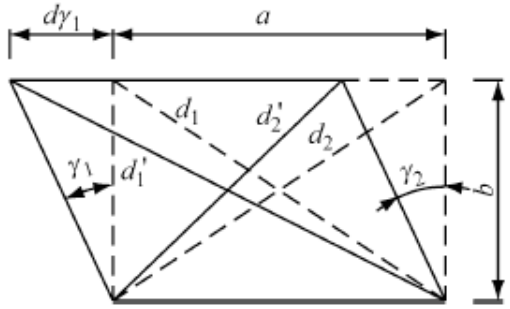

Fig. (6). Geometric graphic of average shearing deformation computation.

5. ANALYSIS OF TEST RESULTS

5.1 Destructive Process and Phenomenon

5.1.1. SRC Specimen SRC

When the loading displacement level is at 10mm and the drift rate is 0.17%, the concrete of specimen SRC starts to crack. Then the crack is concentrated on the range of 2m height from the top face of base. When the yield occurs in the longitudinal bar at the bottom of pier, the displacement level is 40mm and the drift rate is 0.67%. Near the base at southwestern corner of the pier column, a little concrete starts to fall off, the displacement level is at 100mm and the drift rate is 1.67%. But the displacement level is increasingly loaded in order to test the maximum bearing capacity of specimen. The crack occurs, because the loading displacement level of three longitudinal bars at the east of specimen is at 190mm and the drift rate is 3.17%. At the moment, the bearing capacity of specimen descends rapidly till the test is over, as is shown in Fig. (**7A**).

5.1.2. Specimen TRC-SL

When the displacement is at 15mm and the drift rate is 0.25%, the concrete of specimen TRC-SL starts to crack and then the crack is concentrated in the range of 3m height from the top face of base. When the connecting rode S5 (the fifth row starting from the base) starts to yield, the displacement is at 25mm and the drift rate is 0.41%. When the displacement is at 40mm and the drift rate is 0.67, the longitudinal bar starts to yield. When all of the connecting rods start to yield, the displacement is at 80mm and the drift rate is 1.33%. A little concrete in southwestern corner at bottom of west column starts to fall off, the displacement is at 170mm and the drift rate is 2.83%. As is shown in Fig. (**7B**), when the displacement is at 210mm and the drift rate is 3.5%, the connecting rod S5 cracks. The test goes on. As is shown in Fig. (**7C**), when the displacement is loaded at 240mm and the drift rate is 4.00%, four longitudinal bars in east side of eastern column of specimen crack. Then the test is over.

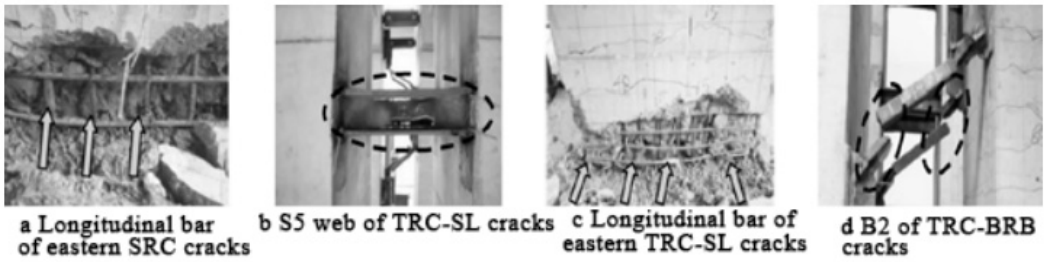

Fig. (7). Destructive forms of specimen.

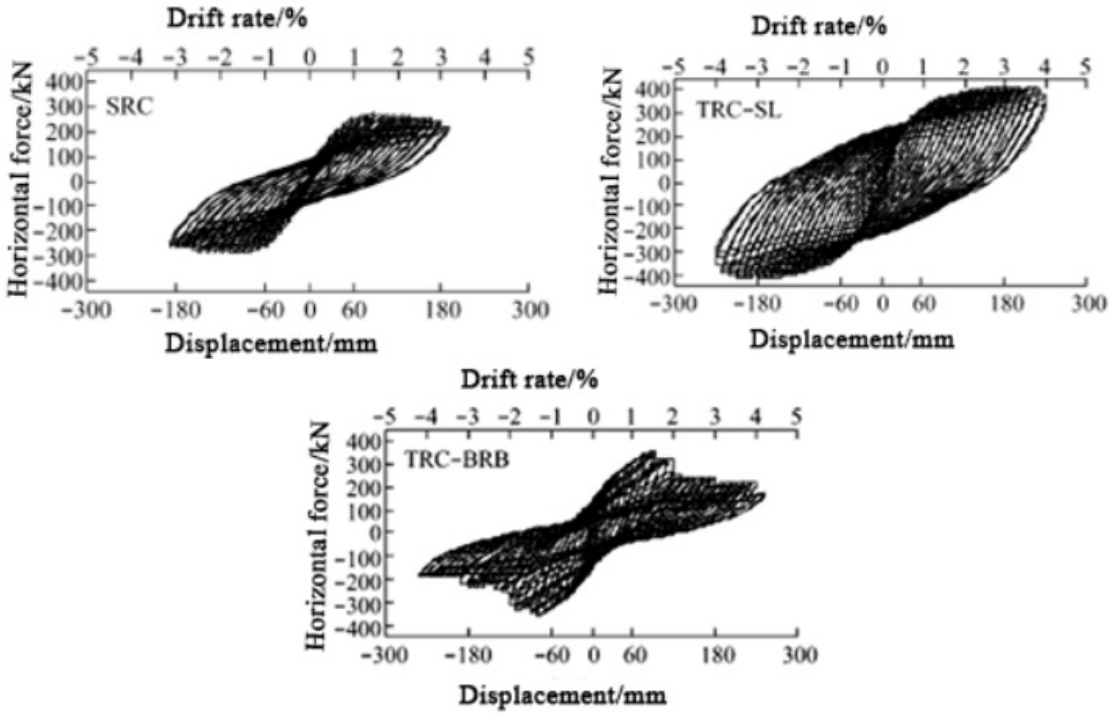

Fig. (8). Hysteretic Curve of Specimen.

5.1.3. Specimen TRC-BRB

When the displacement is at 20mm and the drift rate is 0.33%, the crack starts to occur in specimen TRC-BRB. Then the cracks are concentrated in the range of 3m height from the top face of base, and yield starts to happen in brace B6, B5 and B4 (from the base are respectively the sixth, fifth and forth). When the longitudinal bar yields, the displacement is at 40mm and the drift rate is 0.67%; when all the braces yield, 50mm and 0.67%; when the brace B6 cracks, 120mm and 1.83%; when northern brace of B1 cracks, 190mm and 2.00%; when B2 cracks, 240mm and 4.00% (as is shown in Fig. **7d**). At the moment, the left B4 and southern brace of B1are still bearing while others all crack. But due to the maximum displacement stroke limitation of actuator, the test goes on and it is over when the displacement level is at 250mm and the drift rate is 4.17%. But there is no occurrence that concrete falls off from the protective blanket in bulk.

5.2. Hysteretic Characteristics of Specimen

The seismic performance of specimen is proportional to the plumpness of the hysteretic curve. As is shown in Fig. (**8**), before the concrete starts to crack, the loading and unloading curves overlapped. The hysteretic curve is straight line. Specimen is in the flexible stage. After the concrete cracks, the area of hysteretic loop is gradually enlarged and the hysteretic energy is started. Then the energy dissipation components and longitudinal bars successively yield. The area of hysteretic loop is further enlarged and the capacity of energy dissipation is enhanced. For the double-column specimen TRC-SL and TRC-BRB, the energy dissipation components yield earlier than the longitudinal bar. The double-column pier starts the energy dissipation before the longitudinal bar yields.

5.3. Ductility and Hysteretic Energy of Specimen

In this test, the ultimate displacement of specimen is subject to the displacement when the longitudinal bar of pier column starts to crack. Specific hysteretic energy is calculated by totaling the area surrounded by all hysteretic loops. As is shown in Table **1**, the displacement ductility factor of double-column pier is increased from 5.9 to 12.5, and the hysteretic energy is increased from 1.11MN.m to 4.98MN.m. Compared with the single-column pier, the displacement ductility factor and hysteretic energy of double-column pier is significantly larger, so the energy dissipation components

Table 1. Displacement ductility factor and hysteretic energy of specimen.

Specimen	Yield displacement Δ_y/mm	Yield strength P_y/ k N	Ultimate displacement Δ_m/mm	Ultimate displacement P_m/KN	Maximum displacement ductility factor μΔ	Hysteretic energy ED/ (mN·m)	Maximum drift rate/%
SRC	32.70	185.00	187.90	282.10	5.90	1.11	3.10
TRC-SL	24.80	202.00	239.80	416.40	9.80	4.98	4.10
TRC-BRB	20.00	199.50	249.80	356.20	12.50	2.33	4.20

can greatly improve the seismic performance of the specimen. The displacement ductility factor of specimen TRC-SL is smaller than TRC-BRB, but the hysteretic energy is larger, for the brace is destructed in advance so as to rapidly degenerate the strength and rigidity of specimen TRC-BRB. Thus the displacement ductility factor is increased and the capacity of dissipation energy is decreased.

5.4. Equivalent Viscous Damping Ratio of Specimen

The hysteretic damping of single-column pier and double-column pier is very different. The damping of single-column pier comes from the inelasticity deformation of reinforced concrete, while the damping of double-column pier comes from the inelasticity of dissipation energy components and reinforced concrete. The equivalent viscous damping ratio of single-degree-of-freedom spring oscillator may be used to represent hysteretic damping. The equivalent viscous damping ratio is also the core indicator measuring the capacity of specimen dissipation energy and the indicator is defined as the ratio of monocyclic hysteretic energy to elastic strain energy, as is shown in formula (2).

$$\xi_{eq,h} = \frac{A_h}{2\pi F_m \Delta_m} = \frac{A_h}{4\pi A_e} \quad (2)$$

$$F_m = \frac{1}{2}(|F_{max}| + |F_{min}|) \quad (3)$$

$$\Delta_m = \frac{1}{2}(|\Delta_{max}| + |\Delta_{min}|) \quad (4)$$

In formula (2)-(4): A_h, A_e are respectively the area of hysteretic loop and triangular shadow. Their values equal respectively the weekly hysteretic energy and elastic strain energy, as is shown in Fig. (**9**).

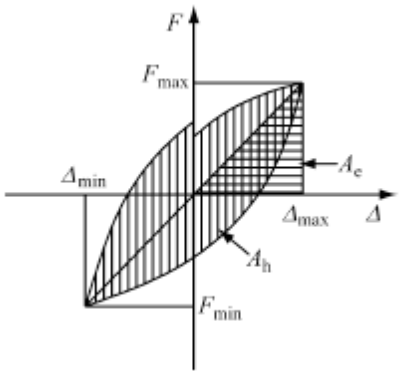

Fig. (9). Hysteretic Energy Dissipation.

As is shown in Fig. (**10**), when the damping ratio is proportional to loading displacement, the specimen TRC-BRB fluctuates more obviously. Due to the failure of brace, when the loading displacement is at 80mm, the damping ratio of specimen TRC-BRB begins to rapidly decrease, finally less than the damping ratio of single-column pier. With the increase of loading displacement, the damping ratio of specimen TRC-SL and SRC increases. Compared to specimen SRC, the maximum damping ratio of specimen TRC-SL is increased by about 44%.

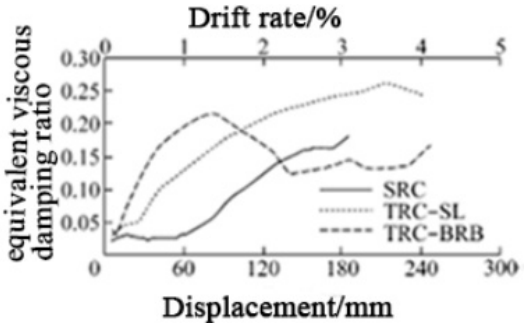

Fig. (10). Changes of equivalent viscous damping ratio when displacement differs.

5.5. Deformation Capacity of Dissipation Energy Components

The shear force of shearing-type connecting rode and axial force of buckling restrained brace can`t be easily measured. It is also difficult to form the hysteretic curve with the same displacement as the force of dissipation energy components, so the horizontal force of pier top is utilized to replace the shear force or axial force of dissipation energy components. The deformation capacity of dissipation energy components can be evaluated by the shearing deformation of pier top horizontal force with dissipation energy components or the hysteretic curve of axial displacement. As is shown in Fig. (**11**), the hysteretic curve of shearing deformation of pier top horizontal force and connecting rode S4 (the forth row from the base), has a plump shape. The maximum shearing deformation is $14\gamma_y$, and the deformation capacity is quite strong. As is shown in Table **2**, the ductility factor of connecting rode next to pier top is the maximum, reaching 20, and the deformation capacity is fully developed. The ductility factor of connecting rode next to pier bottom is quite small, for the relative deformation between the bottom of pier column is quite small.

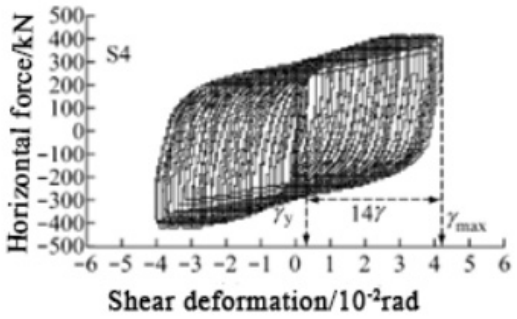

Fig. (11). Hysteretic Curve of Shearing Deformation of Horizontal Force And Connecting Rode S4.

Table 2. Ductility of shearing-type connecting rode.

Shearing-type connecting rode	γ_{max}/rad	γ_{max}/γ_y
S_1	0.010	3
S_2	0.016	4
S_3	0.035	8
S_4	0.042	14
S_5	0.057	20

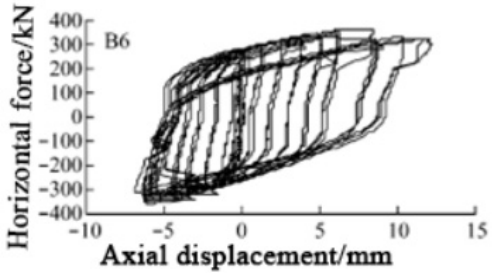

Fig. (12). Hysteretic Curve of Horizontal Force and Axial Displacement of Brace B6.

As is shown in Fig. (**12**), the hysteretic curve of the pier top horizontal force and the axial displacement of brace B6, has a plump shape. But the figure is asymmetric in positive and negative directions, which is quite different from the hysteretic curve of typical buckling restrained brace. The brace can be seen asymmetric in tension-compression direction, as the skeleton curve of specimen TRC-BRB has an asymmetric loading capacity in positive and negative directions. The ductility factors of brace are quite big and the deformation capacity is quite strong. The disadvantage is that the dissipation energy effect can`t go on as the brace is destructed in advance. The ductility factor of brace B4 is the maximum, reaching 38, because brace B4 never cracks in the test.

CONCLUSION

In conclusion, structural damage control may well enhance the safety of the bridge. The internal force and displacement of main components can be reduced correspondingly, so that the safety of long-span cable-stayed bridges is well protected.

CONFLICT OF INTEREST

The authors confirm that this article content has no conflict of interest.

ACKNOWLEDGEMENTS

Declared none.

REFERENCES

[1] J. Xie, "Research on Recognition Methods of Bridge Structure Damage Based on Vibration," *South China University of Technology*, 2003.

[2] J. Wei, "Research on Damping and Vibrational Isolation Measures of Highway-railway Long-span Cable-stayed Bridge," *Lanzhou Jiaotong University*, 2012.

[3] X. Kang, "Research on Damping and Vibrational Isolation and Analysis of Long-span Cable-stayed Bridge Response in Earthquake," *Hefei University of Technology*, 2012.

[4] W. Aiguo, "Analysis on the Dynamic Characteristics and Seismic Performance of Long-span Cable-stayed Bridge," *Wuhan University of Technology*, 2008.

[5] X. Li, "Research on Active Earthquake Response Control of Long-span Cable-stayed Bridge Structure," *Hefei University of Technology*, 2008.

[6] T. A. N. Guan-jun, "The Structure Method and Application of Background Value in Grey System GM (1, 1) Model (I)" *Systems Engineering-Theory & Practice* vol. 4, pp. 018, 2000.

[7] O. Humlum, A. Instanes, and J. L. Sollid, "Permafrost in Svalbard: a review of research history, climatic background and engineering challenges," *Polar Research,* pp. 191-215, 2003.

[8] A. R. Fersht, A. Matouschek, and L. Serrano, "The folding of an enzyme: I. Theory of protein engineering analysis of stability and pathway of protein folding," *Journal of Molecular Biology,* vol. 224, no. 3, pp. 771-782, 1992.

[9] Curtis, and M. Riehle, "Tissue engineering: the biophysical background." *Physics in Medicine and Biology,* vol. 46, no. 4, p. 47, 2001.

[10] L. Sun, W. Jun, and X. Wen, "Experimental Investigation on Energy Dissipation SSubsidiary Subsidiary Piers for Long Span Cable-Stayed Bridges," In*: 15th World Conference on Earthquake Engineering*, 2012.

[11] R. S. Murch, L. Abbott, "Establishing the Quantitative Basis for Sufficiency Thresholds and Metrics for Friction Ridge Pattern Detail and the Foundation for a Standard," *US Department of Justice and National Institute of Justice, Washington DC*, 2012.

Received: February 03, 2015 Revised: April 03, 2015 Accepted: May 25, 2015